Electrical Polarizability of Polyelectrolytes in Salt-free Aqueous Solution

Hitoshi Washizu

Toyota Central R&D Labs., Inc., Nagakute, Aichi 480-1192, Japan

Kazuo Kikuchi*

Department of Life Sciences (Chemistry), Graduate School of Arts and Sciences, The University of Tokyo, Komaba, Meguro-ku, Tokyo 153-8902, Japan

Received: July 10, 2002

Anisotropy of the electrical polarizability $\Delta\alpha$ of model DNA fragments in salt-free aqueous solutions is determined by Monte Carlo simulation. According to the fluctuation−dissipation theorem, the electrical polarizability of polyelectrolytes is related to the fluctuations of the dipole moment generated in the counterion atmosphere around the polyion in the absence of an applied electric field. At every simulation step we numerically sort counterions in increasing order of the sum of their distances from both ends of the polyion. Two kinds of counterions are recognized in distinct spatial distributions, allowing us to give a definition of condensed counterions for charged oligomers based on the simulation. The fraction of condensed counterions so determined approaches Manning's theoretical value as the molecular weight of polyelectrolytes increases. We calculate the contribution to the dipole moment from the first *n* counterions in the sorting list and define a partial polarizability tensor due to these *n* counterions. Its introduction enables us to distinguish between contributions to the polarizability from the two kinds of ions. Contribution from condensed counterions to the radial components of the polarizability tensor is very small as has hitherto often been postulated in various theories. However, contribution from the diffuse ion atmosphere is very large and cannot be neglected in the calculation of the anisotropy. Although in our simulations solvent convection is suppressed, characteristic features of the electric properties of polyelectrolytes in aqueous solutions with no added salt are reproduced. The anisotropy of the electrical polarizability $\Delta\alpha$ of DNA in salt-free aqueous solution increases on dilution of the polymer concentration and is proportional to the second or higher power of the molecular weight. The ∼1 nm thick apparently stable ionic sheath in the immediate vicinity of the polyion should be distinguished from condensed counterions. It is the latter that behaves as a physical entity having characteristic electrical properties.

1. Introduction

Electrical properties of polyelectrolytes in aqueous media have been studied extensively by dielectric dispersion[1−4] and electric birefringence or dichroism.[5,6] Although these highly sensitive techniques have yielded accumulation of data, their theoretical interpretation has been very difficult. A variety of models have been proposed to account for the origin of the induced dipole moment and mechanism of orientation of polyelectrolyte molecules in an applied electric field.

Pollak[7] explained unusually long relaxation times measured in a DNA solution as due to a Maxwell−Wagner mechanism rather than due to the rotation of polarized molecules and gave an expression appropriate for the polarization caused by longitudinal conduction along the molecule. O'Konski[8] introduced a surface conductivity to take into account the excess conductivity arising from mobility of counterions within thin ion atmospheres. Its effect was equivalent to an increased effective volume conductivity of the solute particles in the Maxwell−Wagner polarization treatment. O'Konski and Krause[9] and Krause et al.[10] applied this model to the derivation of equations for the electric field orientation effect of a dilute suspension of ellipsoids of arbitrary and anisotropic volume conductivities and dielectric constants, carrying a dipole.

These theories took a macroscopic approach to describe electrical properties of macromolecules, solvents, and interfaces, and boundary value problems of quasi-electrostatics were solved. To compare theoretical results with experiment, appropriate assignment of the electric parameters was necessary.

Schwarz[11] presented a molecular theory of electrical polarizability of rodlike polyelectrolytes. Counterions were classified into "free and mobile" ions and "bound" ions, the former contributing to the conductivity and the latter being responsible for the polarization. A diffusion equation for the distribution function of the "bound" counterions was solved in the presence of an applied electric field. He also gave a theory of low-frequency dielectric dispersion of spherical colloidal particles in electrolyte solution, taking into account the diffusional relaxation of the counterion distribution along tangential concentration gradients produced by applied electric fields in a conductive surface layer at the sphere-solution boundary.[12] O'Konski[8] neglected this frequency-dependent capacitive part of the surface admittance. Takashima[4,13] extended Schwarz's theory[12] to an ellipsoidal particle. Schurr[14] criticized the boundary conditions employed by Schwarz[12] and derived improved expressions for the dielectric and dielectric loss increments.

These theories neglected interaction forces between counterions, and comparison with experiment required reasonable

* Corresponding author. E-mail: kikuchi@kkc1.c.u-tokyo.ac.jp.

10.1021/jp021581c CCC: $22.00
Published on Web 10/09/2002

values for the density and the mobility of counterions in the double layer.

Mandel[15] calculated the induced dipole moment by an equilibrium statistical mechanical method using a model in which "bound" or "associated" counterions were confined in a one-dimensional square well potential extended longitudinally along the polyion rod axis. Mutual repulsion between counterions was neglected. The relaxation time was calculated by dividing the mean displacement of "bound" counterions by their mean velocity, the latter being expressed using the mobility of ions which might be different from the one for free ions in bulk media. To account for the two (high and low) experimentally observed dispersion regions, the theory was extended to flexible polyelectrolytes modeled as rigid sequences of rodlike subunits of arbitrary but fixed conformation.[16] The effect of the exchange between "associated" and "free" counterions on the induced dipole moment of rodlike polyelectrolytes was also investigated.[17]

According to the fluctuation−dissipation theorem,[18] electrical polarizability of polyelectrolytes is related to the fluctuations of the dipole moment generated in the counterion atmosphere around the polyions in the absence of an applied electric field. Oosawa[19,20] expanded fluctuations in the concentration of "bound" counterions along the polyion rod in a Fourier series and derived real and imaginary parts of the dielectric constant as a sum of contributions from different modes. Schurr[21] criticized Oosawa's theory by pointing out that the self-field associated with the counterion fluctuation was large enough to seriously depress the amplitude of the spontaneous fluctuations. McTague and Gibbs[22] applied a one-dimensional site model for adsorption of counterions and evaluated the partition function by a matrix method from which the mean dipole moment due to counterion perturbation was calculated. Minakata et al.[23] used a similar matrix method to calculate the mean square dipole moment. Warashina and Minakata[24] evaluated the Fourier transform of the counterion−counterion interaction energy in Oosawa's theory[19,20] and found a much smaller reduction of the relaxation time than Schurr found. Minakata[25] further took into account the perpendicular diffusion of counterions from the bulk medium.

All these theories took ion−ion repulsion within the layer of "bound" counterions into account and yielded semiquantitative agreement with experiment by estimating the fraction of "bound" counterions from colligative properties of solutions such as osmotic coefficient values.[26,27]

Vaughan and co-workers[28,29] calculated the dipolar correlation function for a system of counterions diffusing on the surface of a polyelectrolyte cylinder with repulsive Coulombic interactions between them and their lateral dissociation and reassociation to the cylinder taken into account. They found that the correlation function contained a small, fast decaying, molecular weight independent part arising from diffusion around the cylinder and a large, slowly decaying, molecular weight dependent part arising from diffusion along the cylinder axis. They studied the role of the Coulomb forces between the counterions on the dielectric response[30] and on the equilibrium Kerr effect at low[31] and high[32] applied electric fields.

Manning,[33,34] on the basis of his counterion condensation theory,[35−41] derived a formula for the polarizability due to condensed counterions which contained no adjustable parameters as in the previous theories, other than knowledge of the structure of the polyelectrolyte and the ionic strength of the solvent. The polarizability calculated was, however, only weakly dependent on the ionic strength and decreased in the opposite direction to that found experimentally as the ionic strength was decreased, reflecting the increasing stability of the condensed layer.[42]

To account for the experiment, Rau and Charney[43] were the first who pointed out the importance of the contribution to the polarizability of a Debye−Hückel ion atmosphere surrounding the layer of bound or condensed counterions and calculated that it was approximately proportional to the inverse square root of the ionic strength. According to Manning,[44] however, their analysis was not consistent because it retained mixed order terms. Linear analysis[44] showed that for a symmetrical salt, the dipole moment induced in the diffuse ion atmosphere vanished, as the salt ions of one sign prevented polarization of the ions of opposite sign. Rau and Charney[45] also indicated marked saturation properties of the electric polarization of a Debye−Hückel ion atmosphere at high applied electric fields.

To explain the dependence of the dichroism of restriction fragment DNA molecules on the electric field, Hogan et al.[46] proposed a model in which anisotropic ion flow produced an asymmetric ion atmosphere around the polyelectrolyte, resulting in an orienting torque. To incorporate the effect of convective transport of salt ions into theory as one of the sources of the induced dipole moment, Fixman[47] reviewed basic equations of motion of the various fields that should be considered: the concentrations of small ions, the electrical potential, and the solvent velocity. They were coupled with each other through essentially nonlinear equations. He calculated perturbations induced in these fields by the external electric field[47,48] and analyzed numerically the polarizability tensor for short DNA rods in low salt.[49,50]

Recently, Mohanty and Zhao[51] studied polarization of counterions in polyelectrolytes by a density functional method, and Fornés[52−56] published a series of papers calculating the polarizability by a fluctuation−dissipation method in which the colloidal particle with its surrounding ionic atmosphere was considered as a capacitor and a resistor in parallel and the thermal electrical fluctuations across the electrical equivalent were determined.

Despite the voluminous literature briefly reviewed above, our understanding of the electric properties of polyelectrolyte solutions is not in a satisfactory state yet. As pointed out by Fixman,[47] most of the theories do not make a serious effort to describe the solution structure at a fundamental level, for example, by starting with the Smoluchowski mean field approximation which, in zero-field equilibrium, yields the nonlinear Poisson−Boltzmann equation.

In the most basic approach of Fixman and Jagannathan,[50] however, some of our insight was sacrificed.[44] They defined polarizability, for moderate imposed fields, by an asymptotic form of the perturbation in electric potential at large distances from the macroion and expressed it in terms of the polarizability of the gradient of the electrochemical potential of the counterion and its counterpart for the coion.[47] Their variational calculation showed that, for short DNA fragments, longitudinal polarization was smaller than transverse, yielding negative anisotropy as opposed to experiment, unless enhancement of the former by the solvent flow was invoked. According to their model, the outer parts of the ion atmosphere made the dominant contributions and are quite susceptible to convective effects, the calculation of which was of greater difficulty. Also in the linear analysis by Manning,[44] the polarization was isotropic unless the relative motion of macroion and solvent was included.

As we have seen above, the fluctuation−dissipation theorem gives us a simple and clear definition of electrical polarizability. It seems that there remains only to calculate fluctuations of the

dipole moment spontaneously created in the counterion atmosphere without introducing any ad hoc approximations such that counterions are classified as "free" and "bound" ions, nor neglecting interactions between them. For this purpose computer simulation may be useful.

This paper calculates anisotropy of the electrical polarizability $\Delta\alpha$ of model DNA fragments in dilute aqueous salt-free solution by the Metropolis Monte Carlo (MC) Brownian dynamics method.[57−61] Recently we have succeeded in numerical reproduction of the characteristics of the electric properties of polyelectrolytes in both salt-free[62−68] and salt solutions.[67,69]

Electric measurements such as electric birefringence are far more sensitive than other physicochemical methods such as osmotic pressure measurement, allowing us to study very dilute polyelectrolyte solutions. Solution structure of polyelectrolytes involving electrostatic potentials and counterion distributions around polyions have been extensively studied by use of the Poisson−Boltzmann equation,[70−81] hypernetted chain equation,[82] and MC simulation.[83−97] All of these studies, however, approximate polyelectrolyte molecules as infinitely long cylinders and neglect their end effects. On the other hand, as for ionic oligomers there have also been some theoretical[98−104] as well as simulation[105−111] studies. All of these studies, however, treat either added salt systems or much higher polymer concentrations than those used in electrooptic measurements. Structure of salt-free ionic oligomer solutions in a very dilute concentration range has been somewhat shrouded in mystery, and this is one of the reasons why the origin of the induced dipole moment of polyelectrolytes has not been well understood.

The system has prolate spheroidal symmetry with the foci located at both ends of the DNA polyion rod.[112] At every simulation step we numerically sort counterions in increasing order of the sum of their distances from both ends of the polyion. Two kinds of counterions are clearly distinguished in their spatial distributions, even at very dilute polymer concentrations, and are identified, in the framework of counterion condensation theory[20,35] extended to oligomers,[104,113] as condensed ions and those constituting a diffuse or Debye−Hückel ion atmosphere. We define a partial polarizability tensor by calculating fluctuations of the contribution to the dipole moment from the first n counterions in the sorting list. Its introduction enables us to distinguish between contributions to the polarizability from the two kinds of counterions. Contribution from condensed ions to the radial components of the polarizability tensor is very small as has often been postulated in various theories. Contribution from diffuse ion atmospheres is, however, very large and cannot be neglected in the calculation of the anisotropy.

We shall show that condensed counterions are a distinct physical entity characterized not only by their spatial distribution but also by their polarization behavior and that in salt-free solutions the anisotropy of the electrical polarizability $\Delta\alpha$ of model DNA fragments increases on dilution of the polymer concentration and is proportional to more than the second power of the DNA molecular weight, consistent with experiment.

DNA has been occasionally studied in pure water.[114−119] We have extended our simulation study to DNA in salt solution,[69] which has more experimental and biological relevance. However, properties of polyelectrolytes in aqueous solutions with no added salt attract much the same theoretical interest.

2. Simulation

2.1. Method. The Metropolis MC method was originally developed as a numerical method for calculating statistical mechanical configurational integrals by computer.[120] We shall show that the conventional Metropolis MC method, when applied to part of the degrees of freedom of a system, e.g., colloidal particles embedded in a solvent continuum, turns into a simulation procedure of the Brownian motion of the solute particles.

Because the MC sampling is a Markovian process, if we introduce a "time" scale t, which actually labels the order of subsequent configurations X, the "dynamic" evolution of the probability distribution function $P(X, t)$ is governed by the master equation

$$\frac{\partial P(X,t)}{\partial t} = \int [W(X|X')P(X',t) - W(X'|X)P(X,t)]\, dX' \quad (1)$$

where $W(X|X')$ is the transition probability per unit "time" for a transition from configuration X' to X.

The master equation may be solved approximately by an expansion method in powers of a parameter Ω that characterizes the size of the system.[121] Given that $W(X|X')$ has the canonical form

$$W(X|X') = \Phi_0(x';r) + \Omega^{-1}\Phi_1(x';r) + \Omega^{-2}\Phi_2(x';r) + \cdots \quad (2)$$

with $x' = X'/\Omega$ and $r = X - X'$, the jump moments are defined by

$$\alpha_{\nu,\lambda}(x) = \int r^{\nu}\Phi_{\lambda}(x;r)\, dr \quad (3)$$

When $\alpha_{1,0} = 0$, the master equation is of diffusion type and the Ω expansion yields as the lowest approximation a nonlinear Fokker−Planck equation:

$$\frac{\partial P(x,\tau)}{\partial \tau} = -\frac{\partial}{\partial x}\alpha_{1,1}(x)P + \frac{1}{2}\frac{\partial^2}{\partial x^2}\alpha_{2,0}(x)P \quad (4)$$

with $\tau = \Omega^{-2}t$.

In the Metropolis MC, the reciprocal of the maximum displacement allowed for an MC move during "time" interval Δt may be taken as the parameter Ω. Then the transition probability has the canonical form with

$$\Phi_0(x;r) = \frac{1}{2\Delta t} \text{ for } |r| \le 1$$
$$= 0 \text{ for } |r| > 1 \quad (5)$$

and, letting the derivative of the potential energy of the system $U(x)$ with respect to x be $U'(x)$, with

$$\Phi_1(x;r) = -\frac{U'(x)}{2k_B T\Delta t}\left[r - \frac{1}{2}\delta(r)\right]$$
$$\text{for } S(U'(x)) - 1 \le r \le S(U'(x))$$
$$= 0 \text{ for } r < S(U'(x)) - 1 \text{ and } r > S(U'(x)) \quad (6)$$

for sufficiently large Ω; where k_B is the Boltzmann constant, T is the absolute temperature, $\delta(r)$ is the Dirac delta function, and $S(x)$ is the unit-step function:

$$S(x) = 0 \text{ for } x \le 0$$
$$= 1 \text{ for } x > 0 \quad (7)$$

TABLE 1: Simulation Parameters

DNA molecular weight/ (base-pair) N_{bp}	length of DNA /nm	label[a]	radius of MC cell/nm	polymer concentration/ (mM nucleotide residues) c_p	total number of time steps generated[b]
64	21.93	dna1	21.93	4.811	1.024×10^8
		dna2	27.63	2.406	1.280×10^8
		dna3	34.68	1.217	8.192×10^8
		dna4	54.94	0.306	8.192×10^8
128	43.69	dnb1	43.69	1.217	3.712×10^8
		dnb2	55.05	0.609	3.712×10^8
		dnb3	69.22	0.306	3.712×10^8
256	87.21	dnc1	87.21	0.306	2.712×10^8
		dnc2	109.9	0.153	2.712×10^8
		dnc3	138.3	0.077	2.712×10^8

[a] Used in the figures of this article. [b] Calculated by double summing over jobs and nodes.

Equation 6 expresses lowering of the transition probability for a move uphill in energy. From these one obtains

$$\alpha_{1,0} = 0;\ \alpha_{2,0} = \frac{1}{3\Delta t};\ \alpha_{1,1} = -\frac{U'(x)}{6k_BT\Delta t} \tag{8}$$

so that eq 4 reduces to the diffusion equation:

$$\frac{\partial P(x,t)}{\partial t} = \frac{D}{k_BT}\frac{\partial}{\partial x}U'(x)P + D\frac{\partial^2 P}{\partial x^2} \tag{9}$$

where the diffusion constant D is defined by

$$6D\Delta t\Omega^2 = 1 \tag{10}$$

By taking the size of the maximum allowed displacement Ω^{-1} in the Metropolis MC so small that forces acting on a particle remain essentially constant during the MC "time" step, the method switches to a Brownian dynamics simulation.[57,59,60] It was successfully applied to the Brownian motion of a particle under a harmonic potential[57] as well as to the orientation of a dipolar particle in an applied electric field[61] and extended to include hydrodynamic interactions.[58]

It is consistent in principle and convenient in practice to use a single methodology to study both the equilibrium and dynamic properties of a system. We can simulate, for example, relaxation processes of counterion polarization of a polyelectrolyte solution by first preparing equilibrium distribution of counterions around the polyion, then following its change upon application of an external electric field pulse to the solution by the use of the same algorithm.[60]

2.2. Model. The primitive model is used. Fragments of the double-stranded DNA of molecular weight N_{bp} as expressed by the number of base pairs are represented as impenetrable cylinders of radius 0.85 nm with $N = 2N_{bp}$ negative charges spaced at 0.17 nm intervals along their axes. The univalent counterions are modeled as hard spheres of radius 0.15 nm so that the radial distance of closest approach of an ion to the axis of the DNA is 1.0 nm. The cylinders are extended 0.17 nm beyond the terminal charges at both ends. The solvent is treated as a dielectric continuum with the relative permittivity of pure water at 298.15 K and no salt is added. For our DNA oligomers in dilute solutions, the electroneutral cell model[105,122,123] is used for the MC cell. It is a sphere of varying radius in which a DNA fragment is placed along the z-axis with its center in common with that of the sphere or the origin of the coordinate axes. The minimum radius of the sphere is set to the length of the DNA cylinder for each DNA fragment and the DNA concentration is calculated assuming that N nucleotide residues occupy an effective volume the size of the cell which is varied by increasing the radius. Simulation parameters are listed in Table 1. Three fractions of DNA of molecular weight $N_{bp} =$ 64, 128, 256 are studied. Labels shown in column 3 will be used in the subsequent figures of this article.

2.3. Simulation. As explained above, the Metropolis MC is used first to prepare equilibrium distributions of counterions around DNA polyions and then to calculate fluctuations of counterion polarization. According to the cell approximation, the energy of configurations is calculated as a sum of interactions of each small mobile ion in the MC cell with all the other small ions and DNA charges within the cell. Dielectric discontinuity at the solute−solvent interface is neglected, i.e., the dielectric constant is assumed to be uniform throughout the entire MC cell. Ω^{-1} of 0.2 nm is used as the maximum ion displacement allowed for an MC move along each coordinate direction. The new configuration generated by a random move of a single ion is accepted or rejected according to the probability $min\{1, \exp(-\Delta U/k_BT)\}$, where ΔU is the change in configurational energy that would result from the move. When a mobile ion escapes from a peripheral point out of the cell during a move in the Metropolis sampling process, another ion is put to the symmetrical position about the center of the MC sphere. Although the Metropolis time scale Δt is fixed by eq 10, actually we need not relate it to the physical one as far as we calculate time or canonical ensemble averages.

The system has prolate spheroidal symmetry with the foci located at both ends of the DNA polyion rod. At every simulation step we numerically sort counterions in increasing order of the sum of their distances from both ends of the polyion and calculate the contribution to the dipole moment from the first n counterions in the sorting list $(\mu_x(n),\mu_y(n),\mu_z(n))$ as follows:

$$\mu_x(n) = \sum_{i=1}^{n} ex_i$$

$$\mu_y(n) = \sum_{i=1}^{n} ey_i$$

$$\mu_z(n) = \sum_{i=1}^{n} ez_i \tag{11}$$

where e is the protonic charge and (x_i, y_i, z_i) are the coordinates of the ith counterion. We then define the partial polarizability

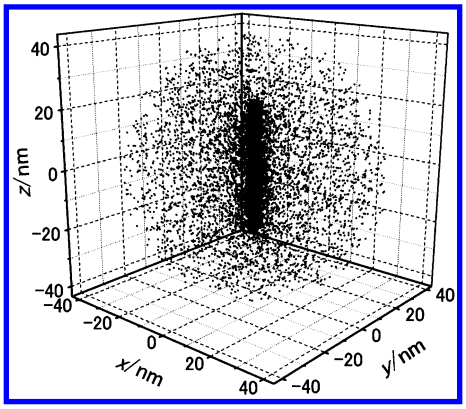

Figure 1. 3D view of the counterion distribution for a $N_{bp} = 128$ base-pair DNA at a polymer concentration $c_p = 1.2$ mM nucleotide residues.

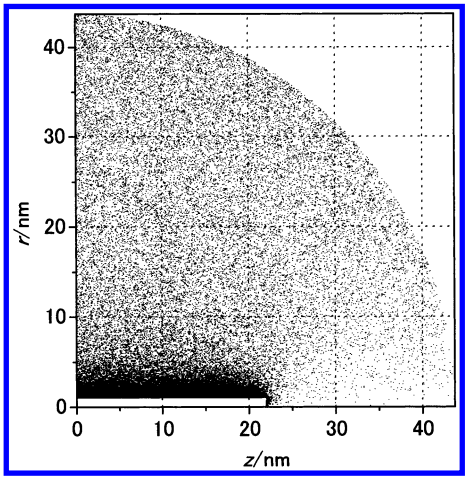

Figure 2. 2D view of the counterion distribution for a $N_{bp} = 128$ base-pair DNA at a polymer concentration $c_p = 1.2$ mM nucleotide residues. Projection of Figure 1 onto a $z-r$ plane where r is the radial coordinate measured from the axis of the DNA cylinder at its center.

tensor due to these n counterions with its principal components $\alpha_{xx}(n)$, $\alpha_{yy}(n)$, $\alpha_{zz}(n)$ given by:

$$\alpha_{xx}(n) = (\langle \mu_x^2(n)\rangle - \langle \mu_x(n)\rangle^2)/k_B T$$

$$\alpha_{yy}(n) = (\langle \mu_y^2(n)\rangle - \langle \mu_y(n)\rangle^2)/k_B T$$

$$\alpha_{zz}(n) = (\langle \mu_z^2(n)\rangle - \langle \mu_z(n)\rangle^2)/k_B T \qquad (12)$$

where $\langle\ \rangle$ denotes time or, as far as equilibrium properties are concerned, canonical ensemble average. The transverse and longitudinal partial polarizabilities, $\alpha_T(n)$ and $\alpha_L(n)$ are defined as

$$\alpha_T(n) = (\alpha_{xx}(n) + \alpha_{yy}(n))/2$$

$$\alpha_L(n) = \alpha_{zz}(n) \qquad (13)$$

and the partial anisotropy of the polarizability $\Delta\alpha(n)$ as

$$\Delta\alpha(n) = \alpha_L(n) - \alpha_T(n) \qquad (14)$$

Here n runs from 1 to N and the anisotropy of the electrical polarizability $\Delta\alpha$ to be determined is expressed as

$$\Delta\alpha = \alpha_L(N) - \alpha_T(N) \qquad (15)$$

Simulations on infinitely long polyelectrolytes ordinarily employ cylindrical cell models neglecting correlations between

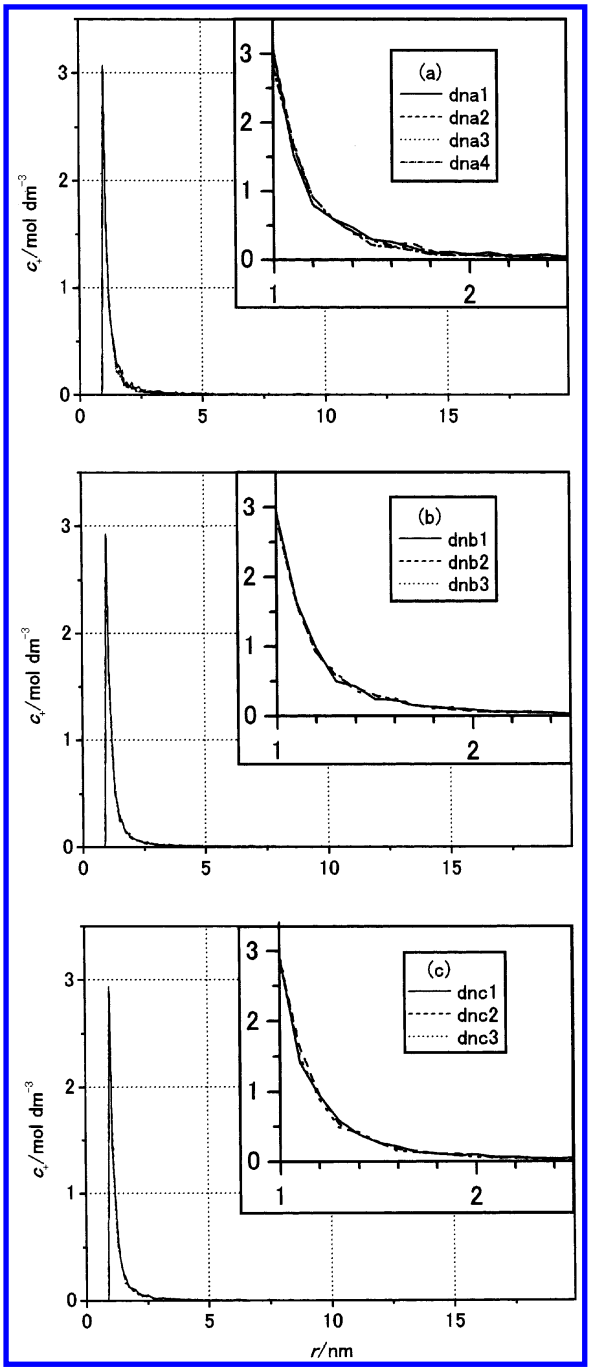

Figure 3. Counterion concentration c_+ profiles for N_{bp} = (a) 64, (b) 128 and (c) 256 base-pair DNA's at various polymer concentrations as functions of the radial coordinate r measured from the axes of the DNA cylinders at their centers.

neighboring polyions. In our dilute finite length polyelectrolyte solutions we extend this approximate treatment to all directions on the assumption that electric fields due to other oligomer ions are shielded on average by their surrounding counterions. Nevertheless, simulations on salt-free dilute solutions still demand large computational resources. The density of a diffuse ion atmosphere is so small in dilute solutions that the determination of each component of the polarizability tensor is not free from statistical errors, i.e., $\Delta\alpha$ is given in eq 15 as a difference of quantities containing large statistical uncertainties.[64] This kind of error can be resolved in the Metropolis MC by averaging over a large number of trajectories. For this purpose, use of the massive parallel Hitachi SR2201 computer of the computer center of the University of Tokyo is indispensable. MC

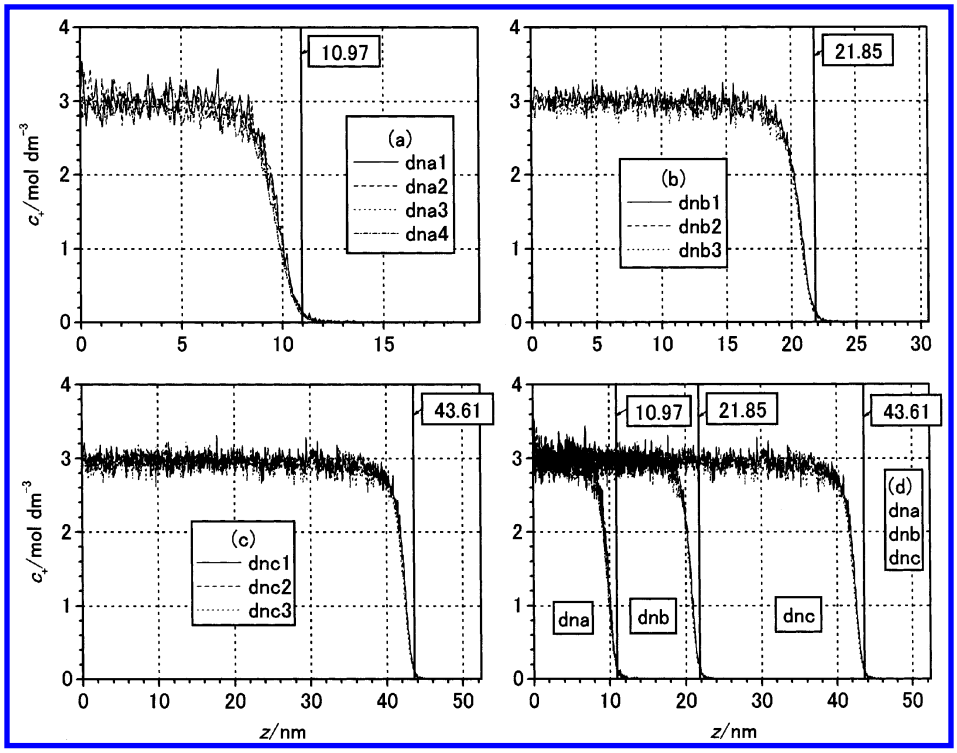

Figure 4. Counterion concentration c_+ profiles for N_{bp} = (a) 64, (b) 128, and (c) 256 base-pair DNA's at various polymer concentrations as functions of the z coordinate along the surfaces of the DNA cylinders. Vertical lines are drawn to indicate terminal positions of DNA cylinders. Part (d) shows all the curves in (a), (b), and (c) superimposed on one another.

simulations are easily parallelized by the use of "embarrassingly parallel" programs which sum up and average over trajectories generated on a large number of nodes. In Table 1, total numbers of simulation time steps obtained by double summing over jobs and nodes are also given.

3. Results

3.1. Counterion Distributions. Figures 1 and 2 show different views of the counterion distribution for a $N_{bp} = 128$ base-pair DNA at a polymer concentration $c_p = 1.2$ mM nucleotide residues. In Figures 1 and 2, a total of 14,000 and 81,920 counterion positions are dotted, respectively. They are collected from uncorrelated configurations generated during the simulation. Two kinds of counterions are recognized in distinct spatial distributions, and prolate spheroidal symmetry of the distribution as well as depletion of the diffuse ion cloud at the ends of the polyion rod is noticed.

To express counterion distributions quantitatively, counterion concentration c_+ profiles are plotted in Figures 3 and 4 for three DNA fragments. Figure 3 shows c_+ profiles at various polymer concentrations as functions of the radial coordinate r measured from the axes of the DNA cylinders at their centers and Figure 4 as functions of z coordinate along the surfaces of the cylinders. The very high counterion concentrations ($\sim$3 M) on the surfaces of the polyions rapidly decrease in both radial and longitudinal directions but dilution of the polymer concentration or DNA molecular weight has little effect on these profiles.

The enormous stability of the $\sim$1 nm thick counterion sheath around DNA observed in these figures has attracted much attention and identification with Manning's condensed counterions has been sought[88,90,91] or debated.[73,81] Because the condensation theory is formulated primarily on polymer models with effectively "infinite" length, if we interpret our simulation data in the framework of the theory, it is necessary to introduce an appropriate definition of ion condensation applicable to oligomers.

Figure 5 shows distances of counterions from polyions or sums of their distances from both ends of the polyions sorted in increasing order and averaged over a number of uncorrelated counterion configurations. In other words, the abscissas are taken as the ordinal numbers n of counterions sorted in increasing order of their distances from the polyions. Note that the ordinates of the graphs start from the values of the lengths of the DNA fragments.

Manning's counterion condensation theory[35] predicts for infinitely long polyelectrolyte chains that 76% of the DNA phosphate charge is neutralized by condensed ions. As Figure 5 shows location of comparable fractions of counterions in the immediate vicinity of the polyions, we are stimulated to look for a proper definition of condensed counterions based on our simulation study.

For each curve in Figure 5 we choose the abscissa where the curve shows the maximum curvature as a unique point separating the two kinds of counterions, condensed and diffuse. Denoting it as n^*, we define the first n^* ions in the sorting list as condensed and the rest as diffuse. Numbers of condensed counterions n^* determined in this way are listed in Table 2, and in Figure 5 vertical line segments are drawn to indicate their positions. Figure 6 shows calculated fractions of condensed counterions for each DNA fragment as a function of polymer concentration c_p.

It is seen that only a few counterions dissociate from the condensed state on dilution. As we have already seen in Figures 3 and 4, polymer concentration has the slightest effect on the concentration profiles of counterions in the immediate vicinity of the polyion. On the other hand, Figure 6 shows that the fraction of condensed counterions approaches Manning's theoretical value as the molecular weight of DNA increases, justifying our definition of ion condensation.

3.2. Electrostatic Potentials. Figure 7 shows $e\psi/k_BT$ profiles at various polymer concentrations where ψ is the electrostatic

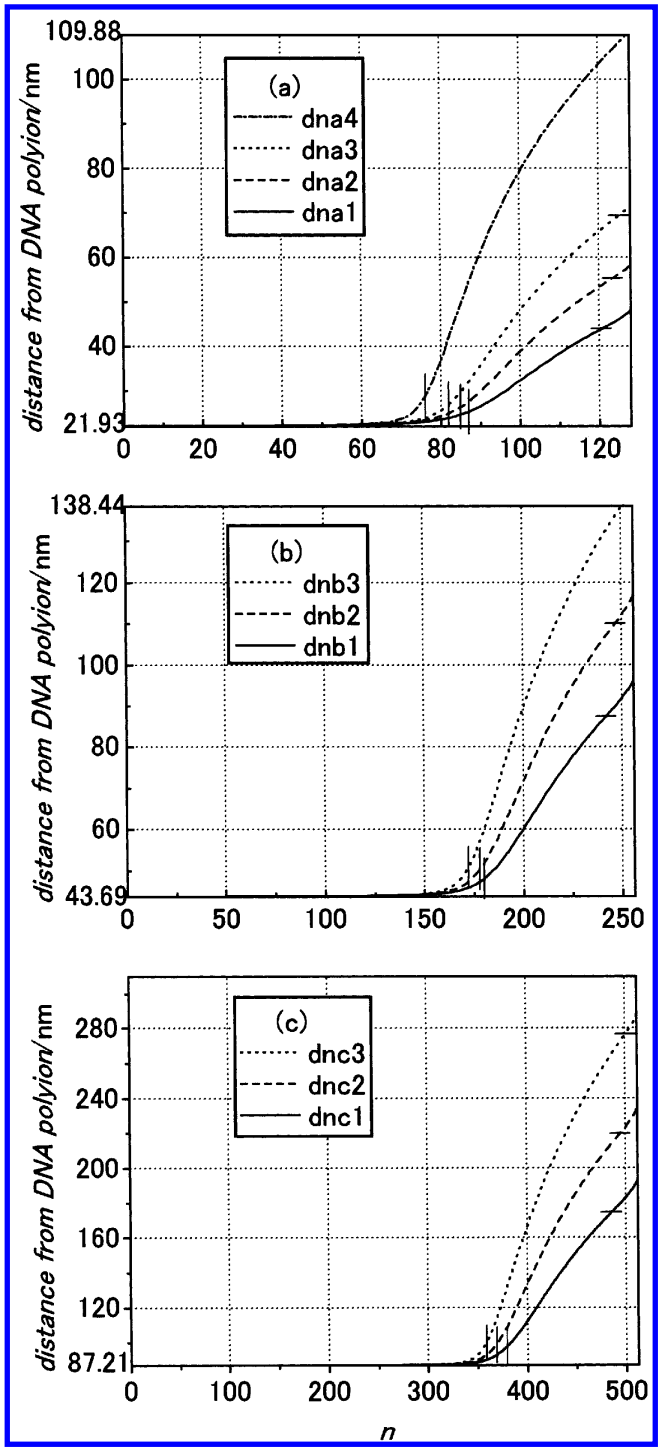

Figure 5. Distance of counterions from N_{bp} = (a) 64, (b) 128, and (c) 256 base-pair DNA polyions or sum of their distances from both ends of the polyions sorted in increasing order and averaged over a number of uncorrelated counterion configurations collected during the simulation. The abscissas are also taken as the ordinal number n of counterions sorted in increasing order of their distance from the polyions. Vertical and horizontal line segments are drawn to indicate points of maximum curvature and diameters of MC cells, respectively.

potential as functions of the radial coordinate r measured from the axes of the DNA cylinders at their centers and Figure 8 as functions of z coordinate along the surfaces of the cylinders. Electric fields due to the polyion are almost completely shielded by the distribution of small ions. A closer look, however, reveals effects of accumulation and depletion of counterions parallel to and at the ends of the polyion, respectively. This tendency of counterions is due to our boundary conditions reflecting

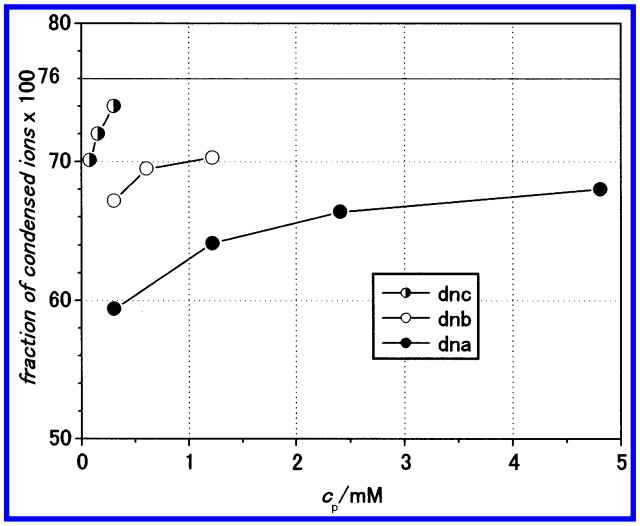

Figure 6. Variations of fractions of condensed counterions for three DNA fragments as functions of polymer concentration c_p.

TABLE 2: Number of Condensed Counterions n^*, Fraction of Condensed Counterions and Positions of Maximum and Minimum Polarizability n_{max}, n_{min} Determined by the Simulation

DNA label	number of condensed counterions n^*	fraction of condensed counterions	position of maximum $\alpha_L(n)$ n_{max}	position of minimum $\alpha_L(n)$ n_{min}
dna1	87	0.68		
dna2	85	0.66		
dna3	82	0.64		
dna4	76	0.59		
dnb1	180	0.703	136	168
dnb2	178	0.695	132	164
dnb3	172	0.672	129	160
dnc1	379	0.74	267	360
dnc2	369	0.72	262	353
dnc3	359	0.701	256	345

parallel disposition of polyions in the neighboring MC cells. The figures also show that the effects of accumulation and depletion of counterions around cell boundaries disappear on dilution. Complete shielding of the polyion fields is attained with very small derivatives of the electrostatic potentials at the cell boundary consistent with our boundary conditions, i.e., neglect of forces from outside of the simulation sphere on average.

In Figure 7, positions corresponding to n^*'s in Figure 5 are marked by vertical line segments. That they look like inflection points of the electrostatic potential curves may be the reason the two-state model has been successfully applied to polyelectrolyte solutions. The inflection points are approximately dividing the solution into two regions: one is occupied by macroions having deep electrostatic potential valleys around them and the other by the rest of the solution with shallow potentials. Figure 9 plots values of reduced electrostatic potentials $e\psi/k_BT$ at the polyion central surfaces as functions of the logarithm of the polymer concentration c_p. The two-state model yields linear dependences of these curves of slope unity.

Figure 8 shows that the effects of the polyion rod ends on the electrostatic potential persist about 3 nm into the interior of the cylinder. We have already seen more amplified end effects on the counterion concentration profiles in Figure 4. In other words, the phosphate charge in these lengths near the ends of DNA fragments is electrostatically more stabilized than that in the interior.

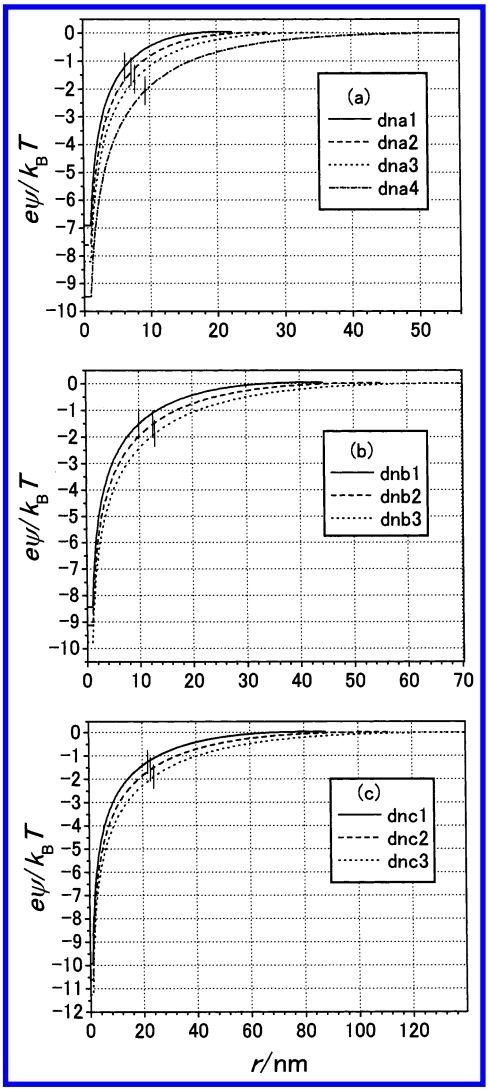

Figure 7. Reduced electrostatic potentials $e\psi/k_BT$ around N_{bp} = (a) 64, (b) 128, and (c) 256 base-pair DNA's at various polymer concentrations plotted as functions of the radial coordinate r measured from the DNA cylinders at their centers. Positions corresponding to n^* are marked by vertical line segments.

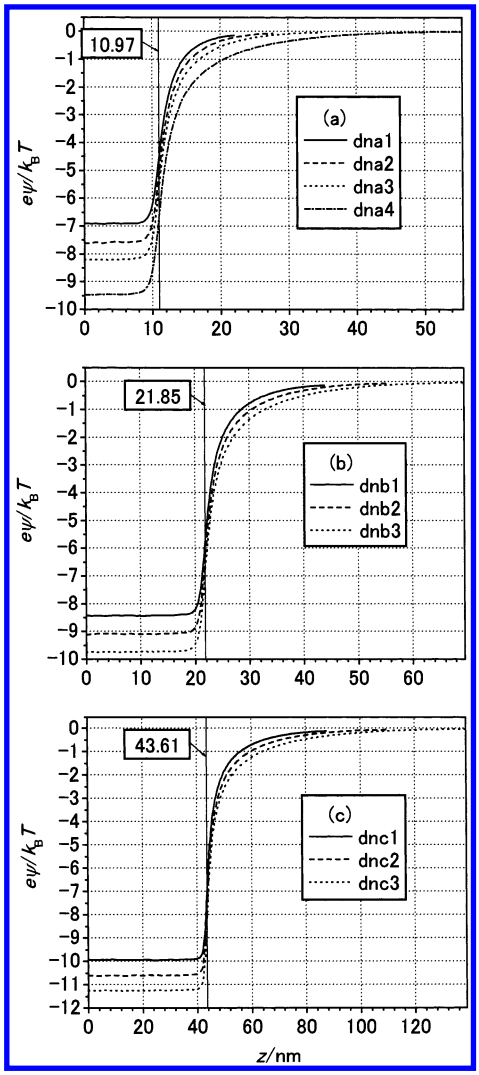

Figure 8. Reduced electrostatic potentials $e\psi/k_BT$ around N_{bp} = (a) 64, (b) 128, and (c) 256 base-pair DNA's at various polymer concentrations plotted as functions of the z coordinate along the surfaces of the DNA cylinders. Vertical lines are drawn to indicate terminal positions of DNA cylinders.

3.3. Electric Polarizabilities. In Figure 10, longitudinal and transverse partial electrical polarizability pairs $\alpha_L(n)$ and $\alpha_T(n)$ determined for each DNA fragment at various polymer concentrations are plotted against the number of contributing counterions n. They are calculated as explained in the previous section. For each pair of curves, the upper one is for $\alpha_L(n)$ and the lower one for $\alpha_T(n)$. In these figures, positions corresponding to n^* as defined above to distinguish between condensed ions and those in a diffuse ion atmosphere are marked by vertical line segments.

The dependence of the partial polarizabilities on n is explained as reflecting the ionic structure in solution. For example, in Figure 10(a), $\alpha_L(n)$ for a 64 base-pair DNA fragment at c_p = 4.8 mM nucleotide residues (labeled "dna1") increases until its phosphate charge is neutralized by about 60 counterions. Since it is calculated by selecting at every simulation step the innermost counterions, fluctuation of the z-component of the partial dipole moment $\mu_z(n)$ increases with n when n is small because the region where selected counterions are distributed in the central part of the polyion expands with n. When the number of the selected counterions increases over 60, fluctuation of $\mu_z(n)$ levels off until n reaches n^*. This is because in this plateau region of the $\alpha_L(n)$ vs n curve, ions to be selected are uniformly distributed along the entire DNA cylinder. When n exceeds n^*, a diffuse ion atmosphere begins to contribute to $\mu_z(n)$, its spatial distribution reflected in the rapidly increasing fluctuation of $\mu_z(n)$.

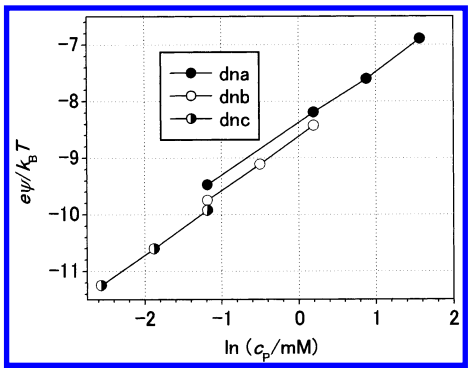

Figure 9. Reduced electrostatic potentials at the surfaces of N_{bp} = (a) 64, (b) 128, and (c) 256 base-pair DNA's $e\psi/k_BT$ plotted against the logarithm of polymer concentration c_p.

Fluctuation of $\mu_x(n)$ and $\mu_y(n)$ remains very small when $n \leq n^*$ because ions are condensed in a layer over the DNA surface.

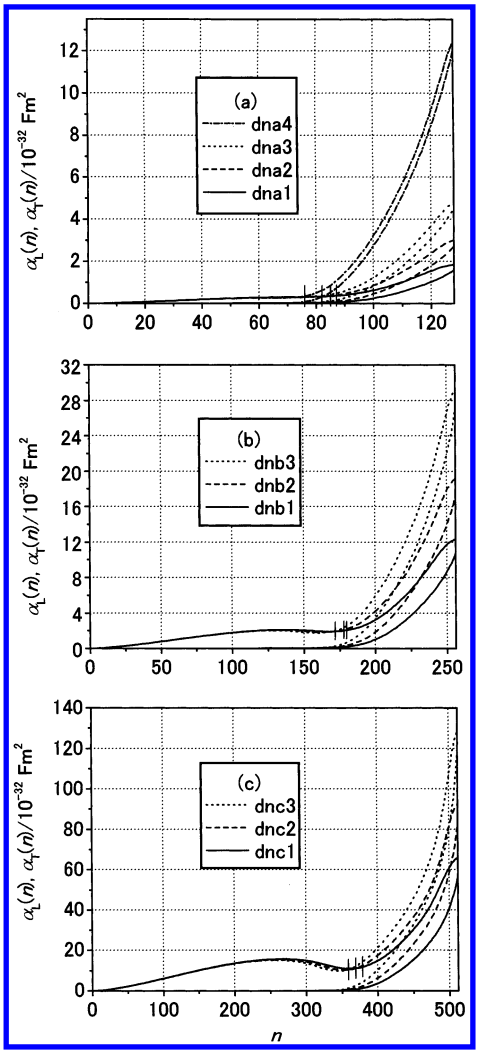

Figure 10. Longitudinal and transverse partial electrical polarizability pairs $\alpha_L(n)$ and $\alpha_T(n)$ determined for N_{bp} = (a) 64, (b) 128, and (c) 256 base-pair DNA's at various polymer concentrations plotted against the number of contributing counterions *n*. For each pair of curves, the upper one is for $\alpha_L(n)$ and the lower one for $\alpha_T(n)$.

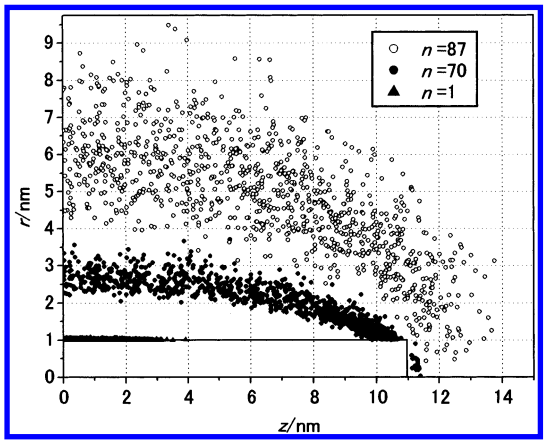

Figure 11. Three distributions of counterions having different distances from a N_{bp} = 64 base-pair DNA cylinder as characterized by the ordinal number n = 1, 70, and 87.

When $n > n^*$, the diffuse ion atmosphere starts to contribute to both $\mu_x(n)$ and $\mu_y(n)$ resulting in their rapidly growing fluctuation. To facilitate visual understanding, Figure 11 shows three representative distributions of counterions characterized by the values of n = 1(innermost), 70 (plateau region) and 87 (= n^*) for "dna1". It looks as if inner distributions contained smaller number of ions only because our graphics program omitted to draw overlapping symbols. It is seen that the innermost layer is very thin sticking to the central part of the polyion where the electrostatic potential is deepest. The 70th distant layer or the group of counterions corresponding to the plateau region of the "dna1" curve in Figure 10(a) extends in fact over the entire rod length. As the distribution of the n^*th distant group or the outer surface of condensed counterions shows, according to our definition, the distribution function of condensed counterions is a smoothly decreasing function of the radial distance *r* and not discontinuously cut off at some jump point.[124]

It is therefore seen that n^* distinguishes not only spatial distributions of the two kinds of ions but also their polarization behaviors. Figure 10(a) also shows that contribution to the polarizability from condensed counterions remains almost constant (on scale expansion it actually slightly decreases) on dilution reflecting their enormous stability[38] while that from a diffuse ion atmosphere increases rapidly.

Figures 10(b) and (c) show similar polarizability curves but they have extra structure in the condensed counterion region. There are a flat maximum and a minimum, and the more marked they are the larger the molecular weight of DNA is. The minimum positions of $\alpha_L(n)$'s are a little smaller than the values of n^* as shown in Table 2. That the partial dipole moment generated in the inner part of the condensation layer is partly canceled out by the opposite polarization of the outer layer might suggest existence of strong correlations such as convective motion within the condensation layer. We cannot, however, afford to pursue more detailed motions of the counterions involved in this paper.

In Figure 12, partial electrical polarizability anisotropies $\Delta\alpha(n)$ determined for each DNA fragment at various polymer concentrations are plotted against the number of contributing counterions *n*. In these figures, we can observe exactly the same regions as in Figure 10 where $\Delta\alpha(n)$'s show different dependence upon *n*. For example, in Figure 12(a) for a 64 base-pair DNA fragment, three regions are distinguished: Region I ($1 \leq n \leq \sim 60$), Region II ($\sim 60 < n \leq n^*$), and Region III ($n^* < n \leq 128$). In Region I, the $\Delta\alpha(n)$ curves rise from 0 until the DNA phosphate charge is neutralized by about 60 counterions. In Region II, they reach plateau values and in Region III, they grow rapidly again. Curves in Figures 12(b) and (c) show similar features with wavy modulation in the condensed counterion regions carried over from Figures 10(b) and (c) and magnified by scale expansion. (Figure 12(c) shows some irregularities of the curves around n = 400 presumably due to the lack of sufficient data accumulation.)

The dependence of $\Delta\alpha(n)$'s on *n* is explained exactly in the same way as above. They show no concentration dependence in Region I consistent with the fact that counterions are strongly bound to the polyion in this region. In Region II, however, they somewhat decrease on dilution. Comparison with Figure 10 indicates that this is the result of the decreased $\alpha_L(n)$ in this region and can be attributed to the deepened electrostatic potential well around the polyion as seen in Figures 7 and 8, i.e., stronger binding forces are exerted on condensed counterions on dilution. In Region III, contribution from diffuse ion atmospheres is added and reversal of the concentration dependence of the $\Delta\alpha(n)$ curves is observed. Their sharp drop in the outer part of this region is due to the boundary conditions of our simulation cell whose effects we can also see on $\alpha_L(n)$

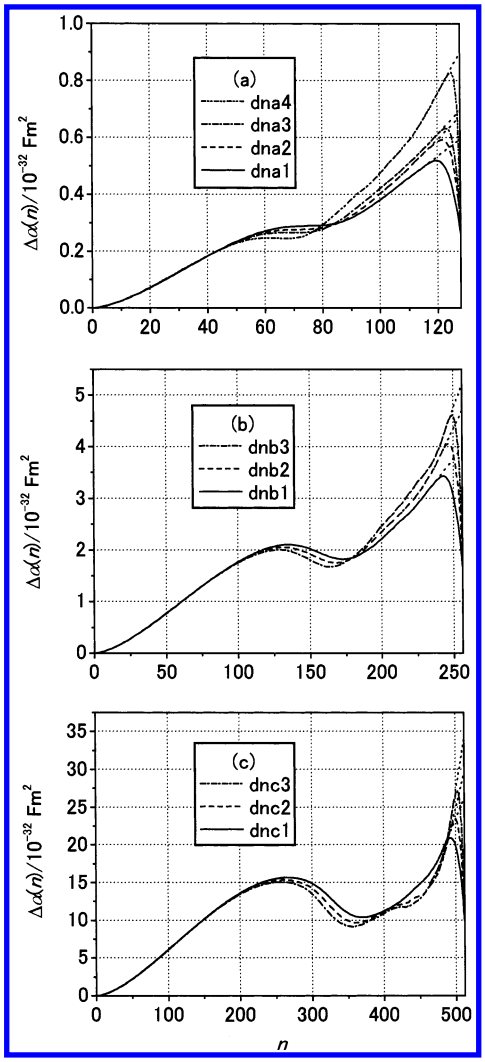

Figure 12. Partial anisotropies of the electrical polarizability $\Delta\alpha(n)$ determined for N_{bp} = (a) 64, (b) 128, and (c) 256 base-pair DNA's at various polymer concentrations plotted against the number of contributing counterions n.

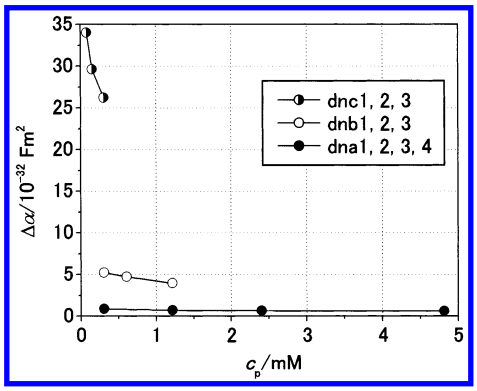

Figure 13. Polymer concentration c_p dependence of the anisotropy of the electrical polarizability $\Delta\alpha$ for N_{bp} = 64, 128, and 256 base-pair DNA's.

curves in Figure 10. Linear portions of the curves are extrapolated to obtain values of $\Delta\alpha(n)$ or $\Delta\alpha$.

Figure 13 shows polymer concentration c_p dependence of the anisotropy of the electrical polarizability $\Delta\alpha$. $\Delta\alpha$ increases on dilution of polymer concentration. Experimentally $\Delta\alpha$ is determined via measurement of the Kerr constant of polyelectrolyte solutions and in the case of rodlike polyelectrolytes both quantities are proportional to each other. It has been observed

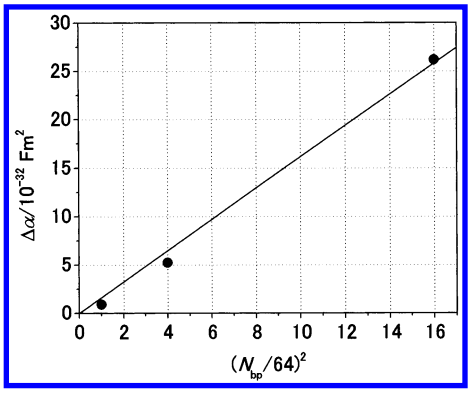

Figure 14. Molecular weight dependence of the anisotropy of the electrical polarizability $\Delta\alpha$ for DNA in pure water at a polymer concentration c_p = 0.31 mM nucleotide residues.

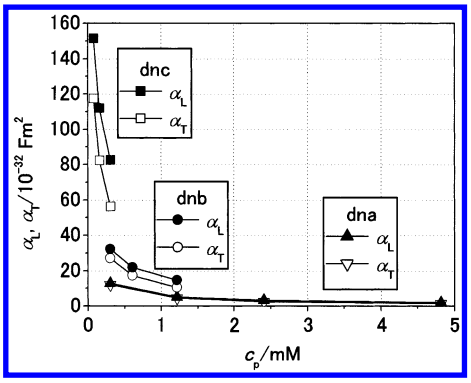

Figure 15. Polymer concentration c_p dependence of the electrical polarizability components α_L and α_T for N_{bp} = 64, 128, and 256 base-pair DNA's.

that the Kerr constant of polyelectrolytes in salt-free aqueous solution increases more sharply on dilution[125,126] the higher the polyelectrolyte molecular weight is.[125]

Strong concentration dependence of $\Delta\alpha$ for high molecular weight polyelectrolyte in salt-free solution makes it difficult to determine its polyion molecular weight dependence, both experimentally and theoretically. It seems that polyion molecular weight dependence has been studied at some fixed polymer concentrations more or less arbitrarily chosen. Figure 14 plots $\Delta\alpha$'s of the three DNA fragments determined at c_p = 0.31 mM against the square of their molecular weight. A linear dependence is observed.

Concentration and molecular weight dependences of the anisotropy of the electrical polarizability have been among the characteristic electrical properties of polyelectrolytes in salt-free aqueous solution that have been experimentally observed but not theoretically explained in a satisfactory way. Figures 13 and 14 show that we have succeeded in their reproduction by computer simulation.

Figure 15 shows polymer concentration c_p dependence of electrical polarizability components $\alpha_L = \alpha_L(N)$ and $\alpha_T = \alpha_T(N)$, and Figure 16 of contributions to them from condensed counterions $\alpha_L(CC) = \alpha_L(n^*)$ and $\alpha_T(CC) = \alpha_T(n^*)$. As Figure 10 shows, since α_L's are influenced by the boundary conditions of the simulation cells whereas α_T's are not so much, the former is calculated as $\alpha_L = \alpha_T + \Delta\alpha$. Figure 16 indicates that contributions from condensed counterions are relatively insensitive to polymer concentration, reflecting their stability. It is therefore concluded that the characteristic concentration dependence of the electrical polarizability of polyelectrolytes is due to the polarization of diffuse ion atmospheres.

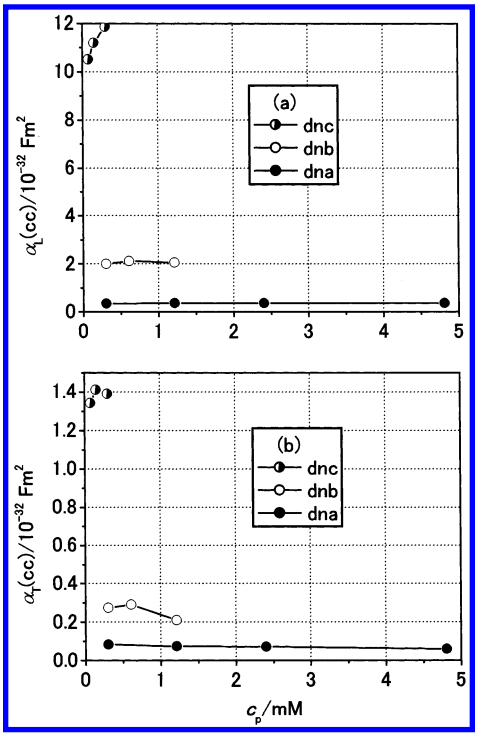

Figure 16. Polymer concentration c_p dependence of the contributions to the longitudinal and transverse electrical polarizability components from condensed counterions (a) $\alpha_L(cc)$ and (b) $\alpha_T(cc)$ for $N_{bp} = 64$, 128, and 256 base-pair DNA's.

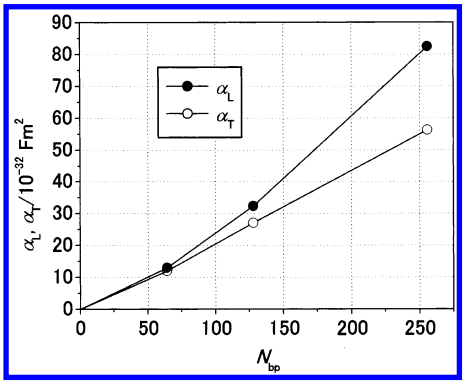

Figure 17. Molecular weight dependence of the electrical polarizability components α_L and α_T for DNA in pure water at a polymer concentration $c_p = 0.31$ mM nucleotide residues.

Figure 17 shows molecular weight dependence of electrical polarizability components α_L and α_T at a polymer concentration $c_p = 0.31$ mM nucleotide residues. The latter is proportional to the first power of DNA molecular weight, whereas the former to the first to second power. Figure 18 shows contributions to the polarizabilities from condensed counterions $\alpha_L(CC)$ and $\alpha_T(CC)$ at the same polymer concentration. They are proportional to the second power of the DNA molecular weight.

4. Discussion

We have studied the origin of the electrical polarizability of polyelectrolytes in salt-free aqueous solution by computer simulation. Correlations between polyions in the very dilute polymer concentration range are neglected using the electroneutral cell model. We have obtained consistent results that polyions are on average completely shielded electrostatically by counterions within their cells.

According to the fluctuation−dissipation theorem, electric polarization of polyelectrolytes is closely related to the equi-

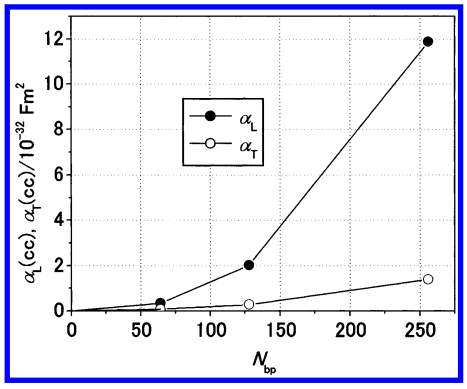

Figure 18. DNA molecular weight dependence of the contributions from condensed counterions to the longitudinal and transverse electrical polarizability components $\alpha_L(cc)$ and $\alpha_T(cc)$ at a polymer concentration $c_p = 0.31$ mM nucleotide residues.

librium solution structure. We have given a definition of condensed counterions for ionic oligomers based on our simulation study. Two kinds of counterions, condensed and the rest forming a diffuse ion atmosphere, are distinguished not only by their spatial distribution but also by their fluctuation or polarization behavior. Contribution from condensed counterions to the radial components of the electrical polarizability tensor is very small as has hitherto often been postulated in various theories. But that from diffuse ion clouds is very large and cannot be neglected in the calculation of the anisotropy. We have succeeded in the computational reproduction of one of the characteristic properties of polyelectrolytes in salt-free solution, i.e., the concentration dependence of the anisotropy of their electrical polarizability.[125,127,128] Its increase on dilution of polymer concentration is a reflection of the structure of diffuse ion clouds and, as Rau and Charney[43] first pointed out, cannot be explained using models which only assume contribution to the polarizability from condensed ions. In salt-free polyelectrolyte solutions, however dilute they are, diffuse ion clouds are so strongly attracted to polyions by the long-range Coulombic forces that they contribute not only to the conductivity but also to the polarizability.

Comparison between simulation and experiment of the molecular weight dependence of the electrical polarizability of polyelectrolytes in salt-free solution is very difficult because of its growing concentration dependence for high molecular weight samples. As for the anisotropy of the electrical polarizability $\Delta\alpha$, first to second power[125] or 2.6 power[128] dependence on the molecular weight has been reported from electric birefringence measurements. Dielectric experiments have yielded first power dependence for the static dielectric increment of polyelectrolytes in pure water[129] and in 10^{-4} N KCl[130] as well as second power dependence in pure water[23,114,115] and in 10^{-3} M NaCl.[131] If we ascribe the static dielectric increment $\Delta\epsilon$ to the longitudinal polarizability of polyelectrolytes α_L, the first power dependence of the former on the molecular weight at a fixed polymer weight concentration is equivalent to the second power dependence of the latter. Although second power dependence of $\Delta\alpha$ is shown in Figure 14, it is evident from Figure 13 that stronger molecular weight dependence will be obtained at lower polymer concentrations. Considering that experimental determination of polarizability is further obscured by molecular flexibility[127] and polydispersity,[128] molecular weight dependence of the electric polarizability of polyelectrolytes in salt-free solutions is not a useful test of a theory.

As we have seen in Figures 4 and 8, since end effects on the counterion concentration as well as the electrostatic potential

TABLE 3: Distances of the Outer Surfaces of the Condensation Layers from the Surfaces of DNA Excluded Volume Cylinders

DNA label	distance/ nm	DNA label	distance/ nm	DNA label	distance/ nm
dna1	5.26	dnb1	8.96	dnc1	20.97
dna2	6.25	dnb2	11.58	dnc2	22.04
dna3	6.78	dnb3	11.96	dnc3	23.26
dna4	8.29				

profiles are limited to relatively small terminal regions of the polyion rods, transverse polarizability α_T is expected to be proportional to the molecular weight and, in fact, Figure 17 shows that this is the case. The long-controversial molecular mechanism for the high frequency dielectric dispersion may be assigned to this counterion fluctuation perpendicular to the polyion axis.[20,25,132] Experimentally, however, stronger molecular weight dependence has been observed.[133] Penafiel and Litovitz[134] studied dielectric properties of Na polyacrylate solutions allowing variation of the charge density across the theoretical critical level for counterion condensation and found the dielectric increment of the high frequency dispersion only above the counterion condensation threshold and therefore linked to the occurrence of counterion condensation. Simulation on the frequency dependence of the electrical polarizability is necessary to study how the distinct polarization behaviors of the two kinds of counterions are related to the two dispersion regions, high and low frequency, observed in these and other dielectric measurements of polyelectrolyte solutions.[2,3]

Le Bret and Zimm[78,135] and Zimm[136] described in detail condensation of the counterions around a highly charged infinitely long cylindrical molecule, such as DNA, in terms of the solutions of the Poisson−Boltzmann equation. They showed that a fraction of counterions only infinitesimally less than the fraction F_M defined by

$$F_M = 1 - 1/\xi \tag{16}$$

where ξ is the linear charge-density parameter of the polyelectrolyte, does not dilute away, even at infinite dilution when $\xi > 1$ (for DNA, $\xi = 4.2$ and $F_M = 0.76$), while the other counterions do. This is a limiting-law definition of condensation and the limiting radius encompassing the fraction F_M of counterions is so large that in practice it looks as if it were expanding indefinitely as polymer concentration approaches zero.

We have shown that fractions of condensed counterions numerically defined for DNA oligomers converge to the Manning fraction $F_M = 0.76$ as their molecular weight increases. It is remarkable that the outer part of the condensed counterions of a charged oligomer keeps distinct polarization behavior, although it is as diffuse as the surrounding innately diffuse ion atmosphere, both receding on dilution of polymer concentration. Table 3 shows distances of the outer surfaces of the condensation layers measured from the surfaces of DNA-excluded volume cylinders (radius 10 nm) at their centers. They depend on the polymer concentration or the radius of the MC cell as electrostatic potential profiles expand on dilution to satisfy the boundary conditions. The ~1 nm thick apparently stable ionic sheath in the immediate vicinity of the polyion[73,81] is just part of the condensation layer. It is not the former but the latter that can be regarded as a physical entity having characteristic electrical properties. Table 3 shows that condensed counterions are trapped within a finite distance of the polyelectrolyte in the concentration range studied by electric birefringence.

In this paper, we used an equilibrium statistical mechanical approach to calculate electric polarizability treating polyions as motionless because of the asymmetry between the diffusion constants of counterions and polyions. Note that it implicitly contains description of solution electrical conductivity in dielectric terms. In our model, counterions on the periphery of the simulation cell where electrostatic potential is zero are free to diffuse independently of other ions because our simulation sphere is not impenetrable. Each of them contributes to the fluctuation of the dipole moment an amount proportional to its position fluctuation, for example, in z direction $\langle z_i^2 \rangle = 2Dt$. Therefore their contribution to the dielectric constant of the system is infinite or they rather contribute to the electric conductivity. Since their distribution is uniform in the peripheral region due to the boundary conditions, their contribution to the dipole moment is, however, counted as zero. When an electric field is applied, an electric current begins to flow in this region and the equilibrium solution structure changes.

Simulation of the polarization of counterions by an external electric field is already performed by us.[137] With the application of an applied electric field, the equilibrium ionic structure is deformed as described above with the peripheral conduction region expanding inward with increasing field strength. The induced dipole moment is, however, proportional to the field strength up to several MV/m.

We have not taken into consideration electrophoretic motion of polyions.[44,47] In this respect, simulation study under an external electric field allowing displacement of both kinds of ions, counterions and polyions, including hydrodynamic interactions between them, is necessary. However, we have already obtained characteristic features of the electric properties of polyelectrolytes in aqueous solution. Anisotropy of the electrical polarizability $\Delta\alpha$ is positive without invoking enhancement of the longitudinal component of the polarizability by the solvent flow. Since an appreciable amount of polyion charge is neutralized by condensed counterions, it is expected that there is some asymmetry not only between the diffusion constants but also between the mobilities of counterions and polyions.

Our simulation study well explains the latest electric birefringence experiment on synthetic polyelectrolytes by Lachenmayer and Oppermann.[138] The concentration and molecular weight dependence of the anisotropy of the electrical polarizability of the stiff-chain charged oligomers are just what we have reproduced for DNA and reported in this paper. The Kerr law behavior is observed up to a field strength of ~1 MV/m. From a comparison of the changes of electric birefringence and electric conductivity upon addition of a low molecular weight electrolyte, the authors attribute the origin of the induced dipole moment of polyelectrolytes to the polarization of diffuse ion atmospheres.

5. Conclusion

We have visualized by computer simulation counterion condensation in dilute aqueous solutions of ionic oligomers with no added salt, and we have clarified the origin of the induced dipole moment of polyelectrolytes in close relation to the ionic structure. Similar studies on added salt systems will be presented in a subsequent paper.

References and Notes

(1) Schwarz, G. *Adv. Mol. Relax. Processes* **1972**, *3*, 281.
(2) Mandel, M.; van der Touw, F. In *Charged and Reactive Polymers*; Sélégny, E., Ed.; D. Reidel: Dordrecht-Holland, 1974; Vol. 1 (Polyelectrolytes); pp 285−300.
(3) Mandel, M.; Odijk, T. *Annu. Rev. Phys. Chem.* **1984**, *35*, 75.

(4) Takashima, S. *Electrical properties of biopolymers and membranes*; Adam Hilger: Bristol, 1989.
(5) *Molecular Electrooptics*; O'Konski, C. T., Ed.; Marcel Dekker: New York, 1976; Part I − Theory and Methods, Part II − Applications to Biopolymers.
(6) Charney, E. Q. *Rev. Biophys.* **1988**, *21*, 1.
(7) Pollak, M. *J. Chem. Phys.* **1965**, *43*, 908.
(8) O'Konski, C. T. *J. Phys. Chem.* **1960**, *64*, 605.
(9) O'Konski, C. T.; Krause, S. *J. Phys. Chem.* **1970**, *74*, 3243.
(10) Krause, S.; Zvilichovsky, B.; Galvin, E. *Biophys. J.* **1980**, *29*, 413.
(11) Schwarz, G. *Z. Physik. Chem. Neue Folge* **1959**, *19*, 286.
(12) Schwarz, G. *J. Phys. Chem.* **1962**, *66*, 2636.
(13) Takashima, S. *Adv. Chem. Ser*. **1967**, *63*, 232.
(14) Schurr, J. M. *J. Phys. Chem.* **1964**, *68*, 2407.
(15) Mandel, M. *Mol. Phys.* **1961**, *4*, 489.
(16) van der Touw, F.; Mandel, M. *Biophys. Chem.* **1974**, *2*, 218.
(17) van Dijk, W.; van der Touw, F.; Mandel, M. *Macromolecules* **1981**, *14*, 792.
(18) Kubo, R. *J. Phys. Soc. Jpn.* **1957**, *12*, 570.
(19) Oosawa, F. *Biopolymers* **1970**, *9*, 677.
(20) Oosawa, F. *Polyelectrolytes*; Marcel Dekker: New York, 1971.
(21) Schurr, J. M. *Biopolymers* **1971**, *10*, 1371.
(22) McTague, J. P.; Gibbs, J. H. *J. Chem. Phys.* **1966**, *44*, 4295.
(23) Minakata, A.; Imai, N.; Oosawa, F. *Biopolymers* **1972**, *11*, 347.
(24) Warashina, A.; Minakata, A. *J. Chem. Phys.* **1973**, *58*, 4743.
(25) Minakata, A. *Ann. N. Y. Acad. Sci*. **1977**, *303*, 107.
(26) Hornick, C.; Weill, G. *Biopolymers* **1971**, *10*, 2345.
(27) Weill, G.; Hornick, C. *Charged and Reactive Polymers*; Sélégny, E., Ed.; D. Reidel: Dordrecht-Holland, 1974; Vol. 1 (Polyelectrolytes), pp 277−284.
(28) Meyer, P. I.; Vaughan, W. E. *Biophys. Chem.* **1980**, *12*, 329.
(29) Meyer, P. I.; Wesenberg, G. E.; Vaughan, W. E. *Biophys. Chem.* **1981**, *13*, 265.
(30) Wesenberg, G. E.; Vaughan, W. E. *Biophys. Chem.* **1983**, *18*, 381.
(31) Altig, J. A.; Wesenberg, G. E.; Vaughan, W. E. *Biophys. Chem.* **1986**, *24*, 221.
(32) Wesenberg, G. E.; Vaughan, W. E. *J. Chem. Phys.* **1987**, *87*, 4240.
(33) Manning, G. S. *Biophys. Chem.* **1978**, *9*, 65.
(34) Manning, G. S. *J. Chem. Phys.* **1993**, *99*, 477.
(35) Manning, G. S. *J. Chem. Phys.* **1969**, *51*, 924.
(36) Manning, G. S. *Annu. Rev. Phys. Chem.* **1972**, *23*, 117.
(37) Manning, G. S. *Charged and Reactive Polymers*; Sélégny, E., Ed.; D. Reidel: Dordrecht-Holland, 1974; Vol. 1 (Polyelectrolytes), pp 9−37.
(38) Manning, G. S. *Biophys. Chem.* **1977**, *7*, 95.
(39) Manning, G. S. *Q. Rev. Biophys*. **1978**, *11*, 179.
(40) Manning, G. S. *Acc. Chem. Res.* **1979**, *12*, 443.
(41) Manning, G. S. *Ber. Bunsen-Ges. Phys. Chem.* **1996**, *100*, 909.
(42) Charney, E.; Yamaoka, K.; Manning, G. S. *Biophys. Chem*. **1980**, *11*, 167.
(43) Rau, D. C.; Charney, E. *Biophys. Chem.* **1981**, *14*, 1.
(44) Manning, G. S. *J. Chem. Phys.* **1989**, *90*, 5704.
(45) Rau, D. C.; Charney, E. *Macromolecules* **1983**, *16*, 1653.
(46) Hogan, M.; Dattagupta, N.; Crothers, D. M. *Proc. Natl. Acad. Sci. U.S.A.* **1978**, *75*, 195.
(47) Fixman, M. *J. Chem. Phys.* **1980**, *72*, 5177.
(48) Fixman, M. *Macromolecules* **1980**, *13*, 711.
(49) Fixman, M. *J. Chem. Phys.* **1981**, *75*, 4040.
(50) Fixman, M.; Jagannathan, S. *J. Chem. Phys.* **1981**, *75*, 4048.
(51) Mohanty, U.; Zhao, Y. *Biopolymers* **1995**, *38*, 377.
(52) Procopio, J.; Fornés, J. A. *Phys. Rev. E* **1995**, *51*, 829.
(53) Fornés, J. A. *J. Colloid Interface Sci.* **1997**, *186*, 829.
(54) Fornés, J. A. *Phys. Rev. E* **1998**, *57*, 2104.
(55) Fornés, J. A. *Phys. Rev. E* **1998**, *57*, 2110.
(56) Fornés, J. A. *J. Colloid Interface Sci.* **2000**, *222*, 97.
(57) Kikuchi, K.; Yoshida, M.; Maekawa, T.; Watanabe, H. *Chem. Phys. Lett.* **1991**, *185*, 335.
(58) Kikuchi, K.; Yoshida, M.; Maekawa, T.; Watanabe, H. *Chem. Phys. Lett.* **1992**, *196*, 57.
(59) Kikuchi, K.; Yoshida, M.; Maekawa, T.; Watanabe, H. In *Colloid and molecular electrooptics 1991*; Jennings, B. R., Stoylov, S. P., Eds.; IOP Publishing: Bristol, 1992; pp 7−12.
(60) Yoshida, M.; Kikuchi, K. *J. Phys. Chem.* **1994**, *98*, 10303.
(61) Yoshida, M.; Kikuchi, K. *Rep. Prog. Polym. Phys. Japan* **1996**, *39*, 115.
(62) Washizu, H.; Kikuchi, K. *Chem. Lett.* **1997**, 651.
(63) Washizu, H.; Kikuchi, K. *Rep. Prog. Polym. Phys. Japan* **1997**, *40*, 597.
(64) Washizu, H.; Kikuchi, K. *Colloids Surfaces A: Physicochem. Eng. Aspects* **1999**, *148*, 107.
(65) Kikuchi, K.; Washizu, H. In *Proceedings of Yamada Conference L: Polyelectrolytes*; Noda, I., Kokufuta, E., Eds.; Yamada Science Foundation: Osaka, 1999; pp 80−81.
(66) Washizu, H.; Kikuchi, K. *Rep. Prog. Polym. Phys. Japan* **1999**, *42*, 367.
(67) Washizu, H.; Kikuchi, K. *Rep. Prog. Polym. Phys. Japan* **2000**, *43*, 615.
(68) Kikuchi, K. In *Physical Chemistry of Polyelectrolytes*; Radeva, Ts., Ed.; Marcel Dekker: New York, 2001; pp 223−243.
(69) Washizu, H.; Kikuchi, K. *Chem. Phys. Lett.* **2000**, *320*, 277.
(70) Fuoss, R. M.; Kachalsky, A.; Lifson, S. *Proc. Natl. Acad. Sci*. **1951**, *37*, 579.
(71) Alfrey, T., Jr.; Berg, P. W.; Morawetz, H. *J. Polym. Sci*. **1951**, *7*, 543.
(72) Stigter, D. *J. Colloid Interface Sci.* **1975**, *53*, 296.
(73) Guéron, M.; Weisbuch, G. *Biopolymers* **1980**, *19*, 353.
(74) Klein, B. K.; Anderson, C. F.; Record, M. T., Jr. *Biopolymers* **1981**, *20*, 2263.
(75) Klein, B. J.; Pack, G. R. *Biopolymers* **1983**, *22*, 2331.
(76) Pack, G. R.; Klein, B. J. *Biopolymers* **1984**, *23*, 2801.
(77) Lamm, G.; Wong, L.; Pack, G. R. *Biopolymers* **1994**, *34*, 227.
(78) Le Bret, M.; Zimm, B. H. *Biopolymers* **1984**, *23*, 287.
(79) Bacquet, R. J.; Rossky, P. J. *J. Phys. Chem.* **1988**, *92*, 3604.
(80) Jayaram, B.; Sharp, K. A.; Honig, B. *Biopolymers* **1989**, *28*, 975.
(81) Rajasekaran, E.; Jayaram, B. *Biopolymers* **1994**, *34*, 443.
(82) Bacquet, R. J.; Rossky, P. J. *J. Phys. Chem.* **1984**, *88*, 2660.
(83) Bratko, D.; Vlachy, V. *Chem. Phys. Lett.* **1982**, *90*, 434.
(84) Bratko, D.; Vlachy, V. *Chem. Phys. Lett.* **1985**, *115*, 294.
(85) Vlachy, V.; Haymet, A. D. *J. Chem. Phys.* **1986**, *84*, 5874.
(86) Le Bret, M.; Zimm, B. H. *Biopolymers* **1984**, *23*, 271.
(87) Conrad, J.; Troll, M.; Zimm, B. H. *Biopolymers* **1988**, *27*, 1711.
(88) Jayaram, B.; Swaminathan, S.; Beveridge, D. L.; Sharp, K.; Honig, B. *Macromolecules* **1990**, *23*, 3156.
(89) Murthy, C. S.; Bacquet, R. J.; Rossky, P. J. *J. Phys. Chem.* **1985**, *89*, 701.
(90) Mills, P.; Anderson, C. F.; Record, M. T., Jr. *J. Phys. Chem*. **1985**, *89*, 3984.
(91) Mills, P.; Paulsen, M. D.; Anderson, C. F.; Record, M. T., Jr. *Chem. Phys. Lett*. **1986**, *129*, 155.
(92) Mills, P.; Anderson, C. F.; Record, M. T., Jr. *J. Phys. Chem*. **1986**, *90*, 6541.
(93) Paulsen, M. D.; Richey, B.; Anderson, C. F.; Record, M. T., Jr. *Chem. Phys. Lett.* **1987**, *139*, 448.
(94) Montoro, J. C. G.; Abascal, J. L. F. *J. Chem. Phys.* **1995**, *103*, 8273.
(95) Montoro, J. C. G.; Abascal, J. L. F. *J. Chem. Phys.* **1998**, *109*, 6200.
(96) Abascal, J. L. F.; Montoro, J. C. G. *J. Chem. Phys.* **2001**, *114*, 4277.
(97) Nishio, T.; Minakata, A. *J. Chem. Phys.* **2000**, *113*, 10784.
(98) Skolnick, J.; Grimmelmann, E. K. *Macromolecules* **1980**, *13*, 335.
(99) Katoh, T.; Ohtsuki, T. *J. Polym. Sci. Polym. Phys. Ed.* **1982**, *20*, 2167.
(100) Satoh, M.; Komiyama, J.; Iijima, T. *Macromolecules* **1985**, *18*, 1195.
(101) Odijk, T. *Physica A* **1991**, *176*, 201.
(102) Allison, S. A. *J. Phys. Chem.* **1994**, *98*, 12091.
(103) González-Mozuelos, P.; de la Cruz, M. O. *J. Chem. Phys.* **1995**, *103*, 3145.
(104) Manning, G. S. *Physica* **1997**, *247*, 196.
(105) Vlachy, V.; Dolar, D. *J. Chem. Phys.* **1982**, *76*, 2010.
(106) Olmsted, M. C.; Anderson, C. F.; Record, M. T., Jr. *Proc. Natl. Acad. Sci. U.S.A.* **1989**, *86*, 7766.
(107) Olmsted, M. C.; Anderson, C. F.; Record, M. T., Jr. *Biopolymers* **1991**, *31*, 1593.
(108) Stein, V. M.; Bond, J. P.; Capp, M. W.; Anderson, C. F.; Record, M. T., Jr. *Biophys. J.* **1995**, *68*, 1063.
(109) Dewey, T. G. *Biopolymers* **1990**, *29*, 1793.
(110) Mills, P. A.; Rashid, A.; James, T. L. *Biopolymers* **1992**, *32*, 1491.
(111) Young, M. A.; Jayaram, B.; Beveridge, D. L. *J. Am. Chem. Soc*. **1997**, *119*, 59.
(112) Kellogg, O. D. *Foundations of potential theory*; Dover: New York, 1954; Chapter 3.
(113) Ramanathan, G. V.; Woodbury, C. P., Jr. *J. Chem. Phys.* **1982**, *77*, 4133.
(114) Takashima, S. *J. Mol. Biol.* **1963**, *7*, 455.
(115) Takashima, S. *J. Phys. Chem.* **1966**, *70*, 1372.
(116) Takashima, S. *Biopolymers* **1966**, *4*, 663.
(117) Tung, M. S.; Molinari, R. J.; Cole, R. H.; Gibbs, J. H. *Biopolymers* **1977**, *16*, 2653.
(118) Vreugdenhil, T.; van der Touw, F.; Mandel, M. *Biophys. Chem.* **1979**, *10*, 67.
(119) Saif, B.; Mohr, R. K.; Montrose, C. J.; Litovitz, T. A. *Biopolymers* **1991**, *31*, 1171.
(120) Metropolis, N.; Rosenbluth, A. W.; Rosenbluth, M. N.; Teller, A. H.; Teller, E. *J. Chem. Phys.* **1953**, *21*, 1087.

(121) van Kampen, N. G. *Stochastic processes in physics and chemistry*, revised and enlarged edition; North-Holland: Amsterdam, 1992; Chapter 11.
(122) Katchalsky, A. *Pure Appl. Chem.* **1971**, *26*, 327.
(123) Linse, P.; Jönsson, B. *J. Chem. Phys.* **1983**, *78*, 3167.
(124) Manning, G. S. *Physica A* **1996**, *231*, 236.
(125) Kikuchi, K.; Yoshioka, K. *J. Phys. Chem.* **1973**, *77*, 2101.
(126) Kikuchi, K.; Yoshioka, K. *Biopolymers* **1973**, *12*, 2667.
(127) Tricot, V. D. M.; Houssier, C.; van der Touw, F. *Biophys. Chem.* **1978**, *8*, 221.
(128) Tricot, M.; Houssier, C. *Macromolecules* **1982**, *15*, 854.
(129) Mandel, M.; Jenard, A. *Trans. Faraday Soc.* **1963**, *59*, 2158.
(130) Molinari, R. J.; Cole, R. H.; Gibbs, J. H. *Biopolymers* **1981**, *20*, 977.
(131) Sakamoto, M.; Hayakawa, R.; Wada, Y. *Biopolymers* **1978**, *17*, 1507.
(132) Cametti, C.; Biasio, A. D. *Macromolecules* **1987**, *20*, 1579.
(133) Ito, K.; Yagi, A.; Ookubo, N.; Hayakawa, R. *Macromolecules* **1990**, *23*, 857.
(134) Penafiel, L. M.; Litovitz, T. A. *J. Chem. Phys.* **1992**, *97*, 559.
(135) Zimm, B. H.; Le Bret, M. *J. Biomol. Struct. Dyn.* **1983**, *1*, 461.
(136) Zimm, B. H. In *Coulombic interactions in macromolecular systems*; Eisenberg, A., Bailey, F. E., Eds.; American Chemical Society: Washington, DC, 1986; pp 212−215.
(137) Yoshida, M.; Kikuchi, K.; Maekawa, T.; Watanabe, H. *J. Phys. Chem.* **1992**, *96*, 2365.
(138) Lachenmayer, K.; Oppermann, W. *J. Chem. Phys.* **2002**, *116*, 392.